New Journal of Physics
The open-access journal for physics

Resistance switching at the nanometre scale in amorphous carbon

Abu Sebastian[1,5], Andrew Pauza[2], Christophe Rossel[1], Robert M Shelby[3], Arantxa Fraile Rodríguez[4,6], Haralampos Pozidis[1] and Evangelos Eleftheriou[1]

[1] IBM Research—Zurich, 8803 Rüschlikon, Switzerland
[2] Plarion Limited, Melbourn Science Park, Melbourn, Herts SG8 6HB, UK
[3] IBM Research—Almaden, 650 Harry Road, San Jose, CA 95120, USA
[4] Swiss Light Source, Paul Scherrer Institut, 5232 Villigen PSI, Switzerland
E-mail: ase@zurich.ibm.com

New Journal of Physics **13** (2011) 013020 (12pp)
Received 23 September 2010
Published 14 January 2011
Online at http://www.njp.org/
doi:10.1088/1367-2630/13/1/013020

Abstract. The electrical transport and resistance switching mechanism in amorphous carbon (a-C) is investigated at the nanoscale. The electrical conduction in a-C thin films is shown to be captured well by a Poole–Frenkel transport model that involves nonisolated traps. Moreover, at high electric fields a field-induced threshold switching phenomenon is observed. The following resistance change is attributed to Joule heating and subsequent localized thermal annealing. We demonstrate that the mechanism is mostly due to clustering of the existing sp^2 sites within the sp^3 matrix. The electrical conduction behaviour, field-induced switching and Joule-heating-induced rearrangement of atomic order resulting in a resistance change are all reminiscent of conventional phase-change memory materials. This suggests the potential of a-C as a similar nonvolatile memory candidate material.

[5] Author to whom any correspondence should be addressed.
[6] Currently at Departament de Física Fonamental and Institut de Nanociència i Nanotecnologia (IN2UB), Universitat de Barcelona, 08028 Barcelona, Spain.

Contents

1. Introduction 2
2. *I–V* measurements on thin-film stacks consisting of amorphous carbon (a-C) 3
3. Electrical transport in a-C 5
4. The permanent resistance-change mechanism in a-C 7
5. Large-scale resistance patterning 10
6. Conclusions 10
Acknowledgments 11
References 11

1. Introduction

Recently, much attention has been focused on the use of various forms of carbon, such as carbon nanotubes and graphene, for nonvolatile memory applications [1]–[3]. However, compared to these forms of carbon, amorphous carbon (a-C) is particularly interesting given the ease with which it can be incorporated into the cell structure of the most promising nonvolatile memory technology, phase-change memory [4, 5]. In fact, in this paper we illustrate the remarkable similarity between the behaviour of a-C and conventional phase-change materials such as germanium antimony telluride (GST).

Carbon exists in multiple forms, the most prominent being the sp^2-dominated graphitic form with its low resistivity and the sp^3-dominated diamond form with its high resistivity [6, 7]. As-deposited a-C has a certain ratio of sp^2 and sp^3 carbon. Changing this ratio can significantly influence the conduction behaviour of carbon. Even for the same sp^3/sp^2 ratio, clustering of sp^2 carbons can lead to enhanced conductivity. The potential for changing the conductivity of a-C at the nanoscale makes it a promising candidate for nonvolatile memory applications. Moreover, the elemental nature of carbon makes a memory device based on carbon scale to very small feature sizes. The deposition techniques will be much simpler. Carbon-based memory devices will be immune to compositional changes that typically plague phase-change memory materials. There is also potential for reduced resistance drift and high levels of data retention. The aforementioned characteristics, along with the high resilience of carbon to a variety of stimuli, make it an attractive material for memory applications.

In previous studies, heat treatment has been shown to change the electrical properties of a-C. By performing bulk annealing, Takai *et al* [8] changed the structure and electronic properties of a-C. They concluded that there is no substantial change in the sp^3–sp^2 ratio up to a temperature of 1100 °C and explained the reduction in resistance during heat treatment at lower temperatures by the clustering of sp^2 carbon. A similar study was conducted by Ferrari *et al* [9] and, more recently, by Grierson *et al* [10]. The application of high electric fields has also been shown to introduce structural changes in a-C. By applying high electric fields locally using a scanning tunnelling microscope probe, Mercer *et al* [11] demonstrated that graphitic nanostructures can be formed on amorphous tetrahedral diamond-like carbon. In these experiments, there is no significant current flowing through the sample and the graphitic formation is assumed to be field induced. Using spatially resolved electron energy

loss spectroscopy, they concluded that the nanostructures arise after an electric-field-induced transformation from predominantly fourfold- to threefold-coordinated carbon.

It has also been shown that the resistance of a-C can be altered by passing current through the material. While studying conduction processes in doped diamond-like carbon films, Ronning *et al* [12] observed a permanent change in resistance. This effect has also been observed by Liu *et al* [13] while designing antifuses, by Tsuchitani *et al* [14] while exploring carbon for probe-based data storage, and by Kostylev *et al* [15] while investigating carbon as a potential electrode material for phase-change memory cells. This means of changing the electrical resistance of a-C is particularly interesting for memory applications. Recently, Kreupl *et al* [16] built a simplistic memory device with a-C and were able to vary the resistance by applying current pulses. The device structure also allowed them to reversibly switch the material between a high and a low resistance state.

In spite of these studies, there is a lack of understanding of the resistance-change mechanism. First of all, given the electrothermal origin of this resistance change, it is essential to establish whether it is field induced or thermally induced. There is also a need to establish whether the mechanism is rehybridization or rearrangement of carbon atoms. Moreover, these investigations have to be conducted at the scale of tens of nanometres that is appropriate for memory applications. Besides the resistance-change mechanism, the conduction mechanism in a-C films needs to be investigated further because it has significant ramifications for properties such as resistance drift and programming voltage, which are critical for nonvolatile memory applications.

In this paper, we present a thorough investigation of the electrical transport and resistance switching in a-C films. Conductive-mode atomic force microscopy (c-AFM) on thin carbon films deposited on conductive bottom electrodes is used in this study. Using this local probe technique, we can switch the resistance of a-C with a spatial resolution of tens of nanometres. c-AFM and our stack configuration also enable the study of the electrical transport mechanism in a-C films across the thickness of these films. Films of varying thickness of a-C and probes with different diameters are employed for this. The effect of thermal annealing is investigated by the application of laser pulses, as well as bulk annealing using rapid thermal annealers. Raman and near-edge x-ray absorption fine structure (NEXAFS) spectroscopy are employed to investigate the resistance-change mechanism. Moreover, the capability of c-AFM probes to pattern large surfaces resistively is demonstrated. This can be exploited for probe-based nano-manufacturing, nano-electronics and probe-based data storage.

2. *I–V* measurements on thin-film stacks consisting of amorphous carbon (a-C)

Resistance switching on a 20 nm thick a-C film is illustrated using the experimental setup shown in figure 1. The setup consists of a home-built AFM with both optical deflection-sensing and conductive-mode operation capability. It is designed such that the micro-cantilevers can be mounted almost parallel to the sample. To create highly localized resistance change, recently developed silicon conductive probes with platinum silicide formed at the apex are employed. These tips can sustain high currents while preserving their nanoscale tip diameter [17, 18].

A film stack consisting of 20 nm of carbon deposited on 40 nm of titanium nitride (TiN) is used. The sample is prepared by first sputtering the conducting layer of TiN onto a silicon substrate. Then carbon is sputtered onto the conducting layer. This stack design is chosen to ensure that the electric field remains normal to the sample surface and across the thickness of

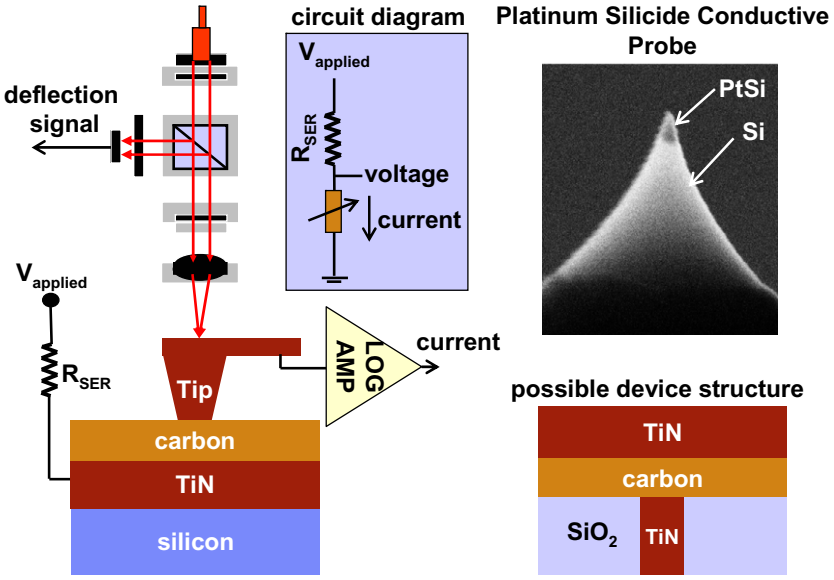

Figure 1. Schematic of the experimental setup to study the electrical transport and resistance-change mechanism in a-C thin films. A conductive probe with nanoscale tip diameter is mounted parallel to a stack of a-C deposited on a conductive substrate. The deflection signal is monitored to maintain a constant tip–sample loading force. The experimental setup is a good emulation of a possible a-C-based memory device (see bottom right).

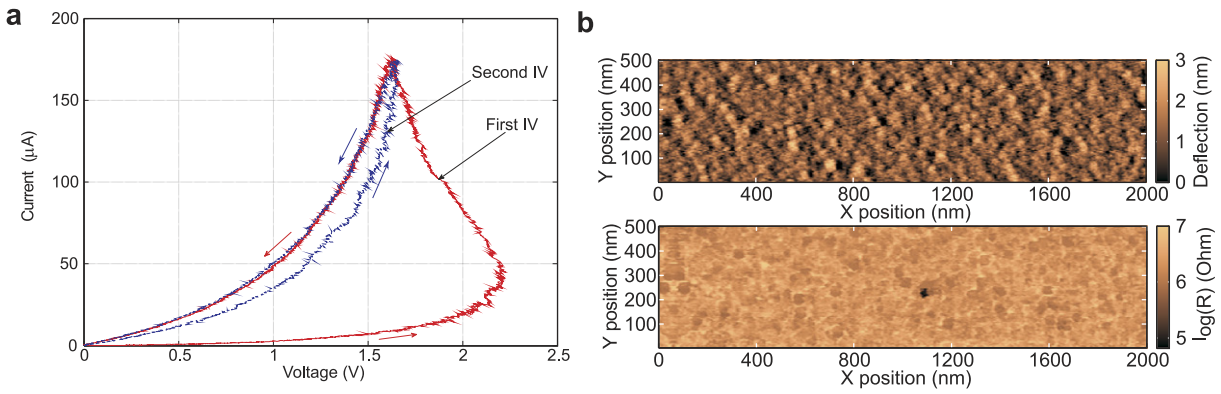

Figure 2. Resistance change in a-C. (a) I–V characteristics obtained on a stack consisting of 20 nm a-C. There is an irreversible change in resistance. (b) Resulting topography (top) and resistance (bottom) maps of the surface.

the film. Carbon is DC sputtered at 4 kW in argon (1.4 Pa, target–substrate distance: 42 mm). Dynamic base pressures of approximately 3×10^{-4} Pa are achieved during the process in the sputtering chamber.

While the tip–sample loading force is maintained at 100 nN, a triangular voltage signal is applied, and the resulting voltage drop across the stack and the resulting current are both measured. This operation is performed twice at the same location. The I–V measurements are shown in figure 2(a). The first I–V measurement exhibits a nonlinear increase in current

as a function of the applied voltage. However, it can be seen that at a certain voltage the resistance drops dramatically. As the voltage is ramped down, a permanent change in resistance is observed. This is also confirmed by the second I–V curve, which follows the return path of the first I–V curve. The topography map and the resistance map of the region are obtained simultaneously (see figure 2(b)). They reveal hardly any change in sample topography, but a significant localized decrease in resistance. The fact that the conductive dot is approximately 20–30 nm in diameter indicates the scaling potential for a-C-based memory devices.

3. Electrical transport in a-C

The electrical transport mechanism is studied first, followed by an in-depth investigation of the permanent resistance-change mechanism. In the first I–V measurement shown in figure 2(a), a switching behaviour is observed at a certain voltage. This phenomenon is called 'threshold switching', and the region of the I–V curve prior to threshold switching is called 'subthreshold conduction regime'. Even though the threshold switching behaviour in a-C has not been reported before, the field-dependent change in resistance observed in the 'subthreshold regime' has been studied by several groups assuming Poole–Frenkel (P–F)-type conduction [19, 20]. The P–F equation for isolated traps is given by

$$I = KV\mathrm{e}^{(-\Phi_\mathrm{B}/k_\mathrm{B}T)}\mathrm{e}^{(q/k_\mathrm{B}T)\sqrt{qV/\pi\epsilon t}}, \tag{1}$$

where K is a constant and Φ_B, k_B, T, q, ϵ and t are the energy barrier at zero field, Boltzmann constant, temperature, elementary charge, dielectric permittivity and thickness of the film, respectively. The experimental I–V curve and the corresponding fit with equation (1) are shown in figure 3(a). It can be seen that the fit is reasonably good, but the extracted relative permittivity value of 112 turns out to be unrealistically high. It is one or two orders of magnitude higher than reported values [21]. A similar observation was also reported by Adkins *et al* [19]. This anomaly is possibly due to the assumption of isolated traps in the P–F conduction model described by 1. If the trap density is high enough such that the mean inter-trap distance is a few nanometres, then the modified P–F model is given by

$$I = K'\mathrm{e}^{(-\Phi_\mathrm{B}/k_\mathrm{B}T)}\sinh\left(\frac{q}{k_\mathrm{B}T}\frac{V\mathrm{d}z}{2t}\right), \tag{2}$$

where K' is a constant and $\mathrm{d}z$ is the average inter-trap distance. In this case, the barrier lowering is mostly independent of the permittivity value and hence does not feature in the equation. The fit of the experimental I–V curve with this model is also shown in figure 3(a). It can be seen that the model in 2 also captures the experimental behaviour as well as the unmodified P–F model. The average inter-trap distance turns out to be approximately 2.2 nm, the smallness of which validates the assumption of high trap density. Moreover, at this value of the mean inter-trap distance, the barrier lowering is mostly independent of the permittivity value. Note that the modified P–F transport model accounting for high trap density has also been proposed by Ielmini and Zhang to describe subthreshold conduction in GST [22].

The threshold switching observed in the I–V measurements occurs prior to the permanent resistance change and is reminiscent of the switching behaviour observed in GST by several groups [22]–[24]. There are strong indications that this threshold switching is field induced. One source of evidence is I–V measurements obtained on stacks comprising varying thicknesses of a-C (see figure 3(b)). The threshold switching voltage increases almost linearly with increasing

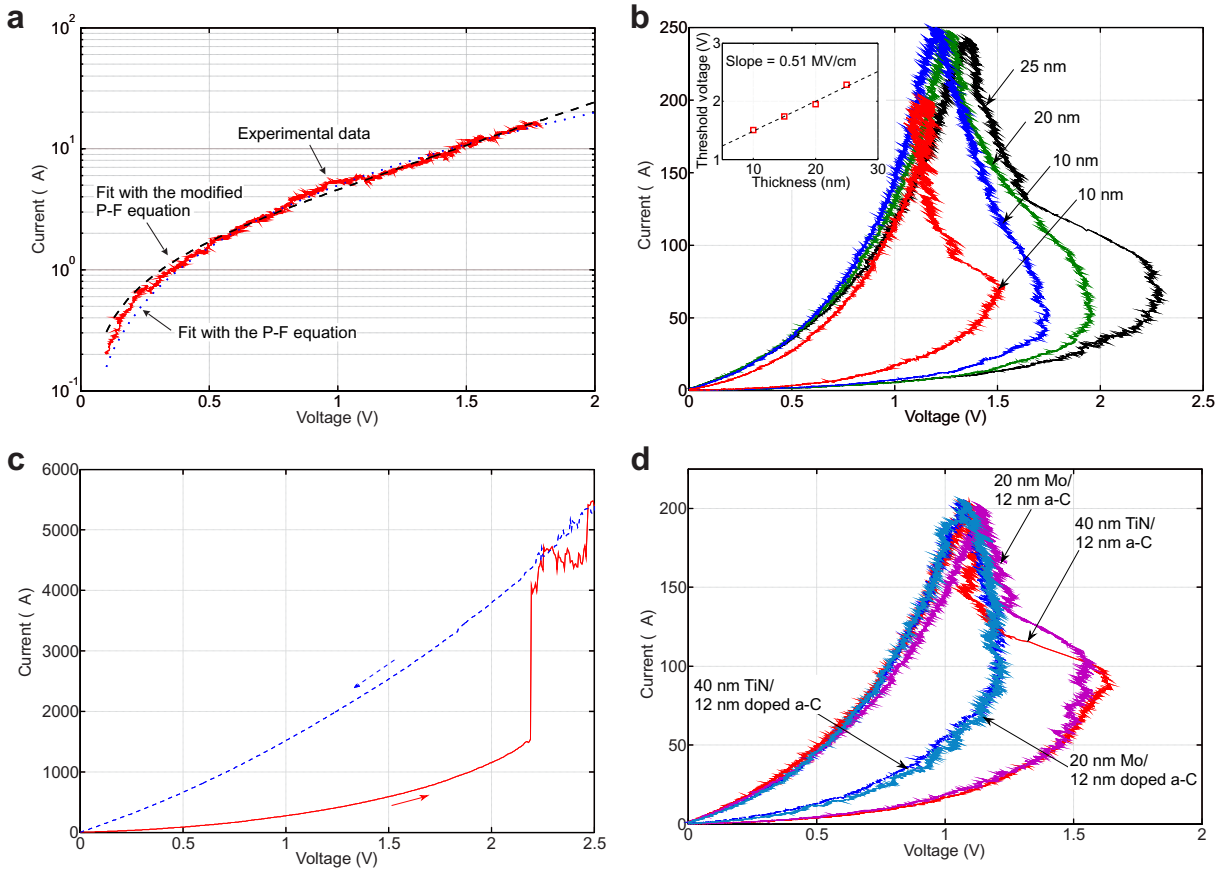

Figure 3. Electrical transport in a-C. (a) Even though both the P–F equation and the modified equation accounting for high trap density fit the 'subthreshold conduction regime' well, the unusually high permittivity values suggest that the latter model is more appropriate. (b) I–V characteristics obtained on stacks with varying thicknesses of a-C. The threshold switching voltage increases almost linearly with increasing thickness of a-C. (c) I–V measurement obtained using a probe with a diameter of more than 1 μm. The threshold switching voltage is mostly independent of the probe diameter, again suggestive of the field-dependent nature of threshold switching. (d) I–V characteristics obtained on stacks consisting of doped and undoped a-C on different bottom substrates. There is no perceivable change in the conduction behaviour as a function of the bottom conductive substrate.

thickness, with a slope of 0.51 MV cm^{-1}. This suggests that the switching mechanism is field induced. I–V measurements were also obtained using probes of varying diameter. An I–V measurement obtained using a probe with a diameter of more than 1 μm is shown in figure 3(c). The stack consists of a 25 nm thick a-C film identical to that shown in figure 3(b). In spite of an order of magnitude increase in current, the threshold switching voltage remains largely unchanged. It is unclear as to which mechanism is responsible for this switching behaviour, but it is clearly field driven, possibly due to tunnelling of carriers from deep traps to shallow traps at high electric fields. From these studies, it can be seen that the subthreshold conduction behaviour and threshold switching are remarkably similar to that observed in GST.

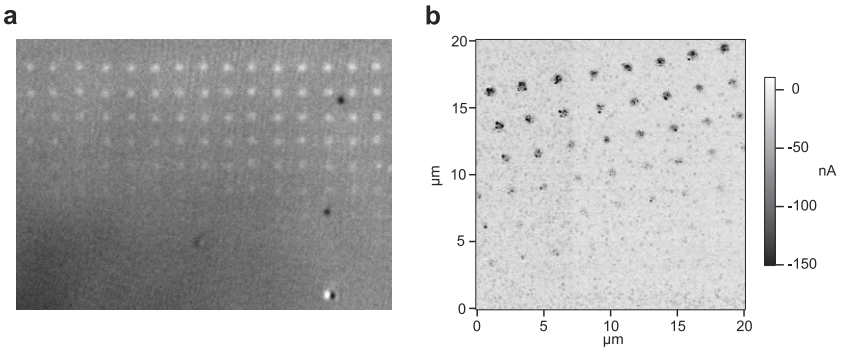

Figure 4. Resistance change using laser pulses. (a) Optical micrograph obtained after the application of laser pulses with varying duration and power, showing increased reflectivity of the most intensely heated spots (upper right corner of the array, corresponding to a maximum laser power of 55 mW and a pulse duration of 100 μs). The spacing between adjacent spots is 2.5 μm. The largest relative reflectivity increase observed was $\sim$7%. (b) c-AFM image of the top central portion of the array shown in (a), demonstrating increased conductance of the heated spots for a laser power in the range 25–55 mW and pulse durations of 1–10 μs. Sample bias was -7 mV, and a solid Pt metal probe was used for this image.

It is essential to rule out the impact of the bottom conductive layer on the electrical transport mechanism. Hence experiments were performed on two different stacks, one having a 40 nm thick layer of TiN as bottom electrode and the other having a 20 nm thick layer of molybdenum as bottom electrode. These materials were chosen because of the significant difference in their electrical conductivity. Both doped (nitrogen) and undoped a-C films were prepared using these stacks. The I–V curves obtained on these four stack configurations are shown in figure 3(d). There seems to be no perceivable difference in the conduction behaviour. The higher current values prior to threshold switching in the doped-carbon stack are indicative of a reduced energy barrier for hopping due to nitrogen doping [6].

4. The permanent resistance-change mechanism in a-C

The permanent resistance switching mechanism is investigated next. First it is shown by means of a focused laser beam that a resistance change can be induced by local heating alone without electrical excitation. A film stack consisting of 50 nm of carbon deposited on 40 nm of TiN on a silicon substrate was heated by 658 nm wavelength laser pulses of varying duration and laser power, focused to a 1 μm diameter spot. The reflectivity of the sample was monitored after each pulse using a low-power, continuous 630 nm laser beam focused onto the same place on the sample. The sample was translated by 2.5 μm between pulses, producing an array of laser-heated spots in which the pulse width and laser power varied from 10 ns to 100 μs and from 10 to 55 mW, in the horizontal and vertical directions, respectively. We estimate that about half the laser power is absorbed by the carbon film, about 15% reflected and the remainder absorbed in the TiN. Figure 4(a) shows an optical microscopy image of a part of the resulting array of spots for pulse durations increasing geometrically from 1 μs on the left to 100 μs on the right, and linearly from 10 mW at the bottom to 55 mW at the top. For laser pulses of $\sim$30 mW or more and durations greater than $\sim$30 ns, an increase in the relative optical reflectivity is

observed, reaching about 7% at the highest power and largest pulse width. This localized laser heating also induced a decrease in the resistance of the film, as revealed by a c-AFM scan of the spot array shown in figure 4(b). The resistance of the heated spots was decreased by approximately an order of magnitude compared with that of the surrounding unheated area. A similar study has been reported in [25], where a-C deposited using pulsed-laser-deposition technique is used. Resistance change while maintaining surface smoothness is observed. The findings presented in this paper are consistent with our studies.

The laser experiments clearly show that local heating can result in a local decrease in resistance and suggest that Joule heating is a significant contributor to the permanent resistance change described earlier. In case the resistance change is due to Joule heating, then it is useful to have an estimate of the temperatures that have been reached during the resistance-change process. This will also help identify the resistance-change mechanism. Therefore, an experiment was performed in which film stacks consisting of 50 nm of carbon deposited on 40 nm of TiN on a silicon substrate were annealed at different temperatures for 5 min in an argon environment. I–V curves were obtained at room temperature on these samples after the annealing step (see figure 5(a)). From the I–V curves obtained while the voltage is being ramped up, it can be seen that there is a steady decrease in resistance as the annealing temperature is increased. Comparison of these curves with the I–V curve corresponding to the electrothermally induced resistance change of the unannealed sample shows that the resistance change obtained by electrothermal means is comparable to the annealed sample at temperatures between 300 and 400 °C. At these low temperatures, it is highly unlikely that there is any conversion of sp^3 to sp^2 sites [8, 9]. So, if the resistance change is mostly due to Joule heating, then it is likely that the resistance change is caused by the clustering of existing sp^2 sites.

Raman spectroscopy can help validate this clustering assumption [9, 26]. Raman spectra were excited at 532 nm using a micro-Raman setup with a laser spot size of about 1.5 μm. Raman spectra were obtained on the thermally annealed samples and also on a pattern created using electrothermal means. Raman spectra of as-deposited films show broad G and D bands of comparable relative intensity, with a G-band peak at 1548 cm^{-1}. This suggests that a large percentage of the carbon is sp^2-bonded, with a significant degree of clustering of sp^2 carbon to form graphitic-like regions. Using equation (12) in [26], we can estimate the size of the clusters from the Raman spectra. The initial intensity ratio is 0.68, which corresponds to an average cluster diameter of 1.1 nm. We have investigated the changes in the Raman spectra upon annealing and electrothermal or pulsed laser patterning. The spectra were fit to a two-peak model consisting of a Lorenzian lineshape for the D-band and a Breit–Wigner–Fano lineshape for the G-band [8, 9, 26]. Figure 5(b) shows the resulting G-band frequency and the D to G-band peak intensity ratio for the as-deposited film, films annealed to 300–700 °C and an electrothermally modified region of one of the films. The electrothermally modified regions were rectangular and had dimensions of 4 μm × 10 μm. They were created by applying several write pulses over the whole region. Large-scale patterning of surfaces is presented in more detail in section 5.

Both thermal annealing and electrothermal patterning produce a shift of the G-band to higher frequency and an increase in the relative D-band intensity. This is consistent with an increase in the average size of the graphitic sp^2 clusters, because in this regime I_D/I_G is thought to be approximately proportional to the square of the size of such clusters. The clustering is accompanied by a decrease in the optical band gap [8, 26]. This occurs at relatively low temperatures, consistent with our suggestion that the predominant process is an increase in the

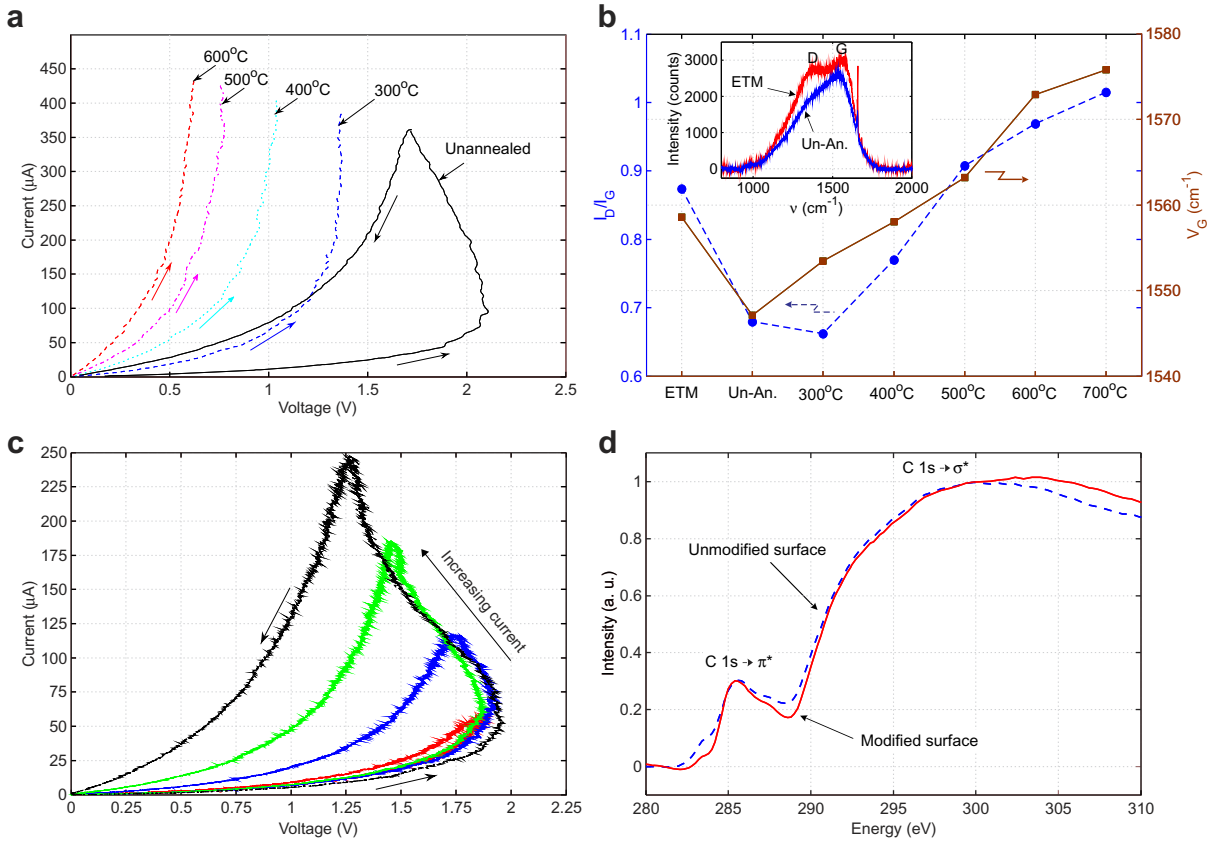

Figure 5. The permanent resistance-change mechanism. (a) I–V curves obtained at room temperature on annealed a-C stacks compared with an electrothermal switching at room temperature. (b) Variation of G-band peak positions (squares) and I_D/I_G peak intensity ratios (circles) from the visible Raman spectra obtained from thermally annealed samples (300–700°C), unannealed (Un-An.) and electrothermally modified (ETM) samples. In the inset, the Raman spectrum obtained from the electrothermally modified sample is compared with that obtained from the unannealed sample. (c) I–V characteristics obtained with increasing values of current on a stack consisting of 20 nm a-C. There is a direct correlation between the extent of resistance change and the applied power. (d) Comparison of the NEXAFS spectra of the a-C film inside and outside an electrothermally modified area. The ratio of the areas under the C 1s $\rightarrow$ π^* and C 1s $\rightarrow$ σ^* resonances remains largely unchanged.

average size of sp^2 clusters rather than sp^3 to sp^2 conversion. The increase in I_D/I_G ratio and in the G-band peak position for the electrothermally modified sample similar in magnitude to those for thermally annealed samples at 400–500 °C, which is remarkably close to the estimate from the I–V measurements presented earlier.

In figure 5(c), experimental results are presented in which resistance change is obtained with increasing current amplitudes. It can be seen that the extent of resistance change increases with increasing current and the corresponding increase in power. This is also suggestive of the resistance-change mechanism being induced by Joule heating. It has significant ramifications for multi-level storage in the context of memory applications.

Given the electrothermal nature of resistance switching, there could be some sp^3 to sp^2 conversion due to the high fields that are generated within the carbon film. NEXAFS spectra of the as-deposited a-C film and the electrothermally modified surface were obtained to investigate this possibility. The NEXAFS spectra were obtained using a photoemission electron microscope (PEEM) in ultra-high vacuum conditions. The laterally resolved NEXAFS experiments were performed at the surface/interface:microscopy beamline of the Swiss Light Source, using an Elmitec PEEM equipped with an energy analyzer. Several NEXAFS spectra were obtained inside and outside an electrothermally modified area and the average of these spectra is shown in figure 5(d). The peak at around 285.5 eV is due to the C 1s $\rightarrow \pi^*$ transition for disordered carbon–carbon sp^2-hybridized bonds and a broad peak starting above 288 eV and extending up to 305 eV is due to the C 1s $\rightarrow \sigma^*$ transition for disordered carbon–carbon σ bonds. The similarity between the two curves suggests that the sp^3–sp^2 ratio remains largely unchanged. The ratio of the area under the C 1s $\rightarrow \pi^*$ and C 1s $\rightarrow \sigma^*$ resonances would have changed significantly if there was a change in the sp^3–sp^2 ratio [10]. Hence from all these results, it is established that the resistance change is caused by Joule-heating-induced clustering of existing sp^2 sites, or in other words the rearrangement of sp^2 carbon atoms within the sp^3 matrix, as opposed to any significant rehybridization of the carbon atoms.

5. Large-scale resistance patterning

Besides memory applications, the capability of conductive probes to create highly localized resistance change on a-C thin films can be exploited for applications such as probe-based nano-manufacturing, nano-electronics and probe-based data storage [27]–[30]. To study the potential for large-scale resistance patterning at the nanoscale, a large pattern consisting of approximately 5000 write pulses was written using the platinum silicide conductive probes on a stack consisting of 50 nm of carbon film on 40 nm of TiN. The resulting topography and conduction maps are shown in figure 6. It can be seen that there is no appreciable change in the sample topography; however, there is a significant change in resistance. This experiment clearly demonstrates the capability of conductive probes to resistively pattern large areas of a-C films with high throughput.

6. Conclusions

The electrical transport and resistance-change mechanisms in thin a-C films are investigated. It is demonstrated that we can locally switch the resistance of these films down to tens of nanometres using c-AFM probes. Newly developed platinum silicide conductive probes which can sustain high currents while maintaining a small tip diameter were employed.

A P–F-type transport model that accounts for nonisolated traps describes the electrical transport up to a certain electric field well, at which point there is evidence of a threshold switching behaviour. This results in a significant increase in the current flowing through the sample and subsequent Joule heating, which results in a permanent resistance drop. The thermal origins of this resistance change are firmly established by laser-pulse-induced resistance patterning and bulk annealing studies. Raman spectroscopy and NEXAFS spectroscopy allow us to conclude that the resistance change is caused by the clustering of existing sp^2 sites within the sp^3 matrix.

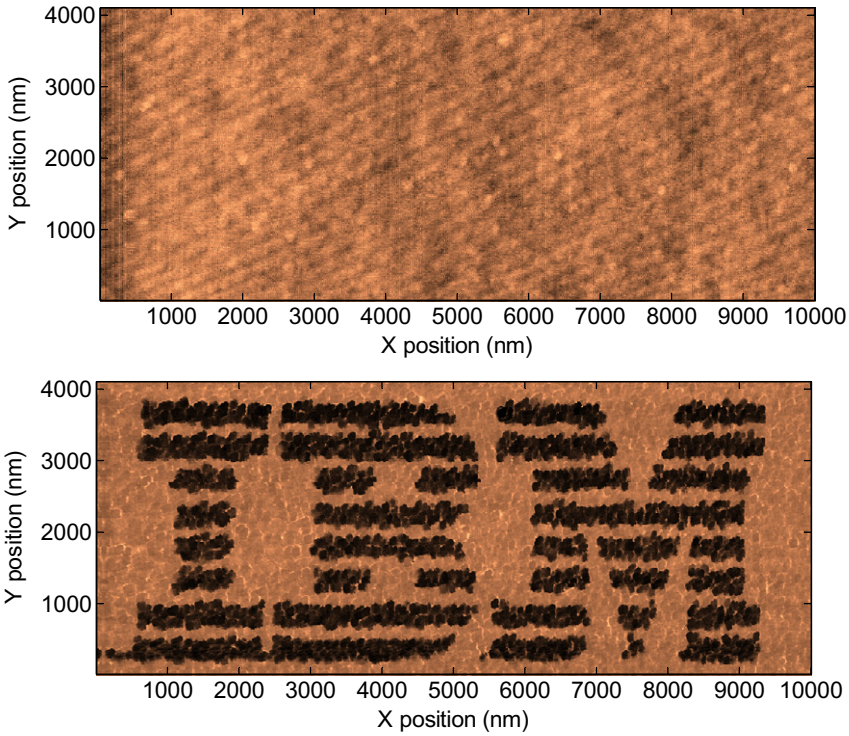

Figure 6. Large-scale resistance patterning of a-C. The pattern is created by applying several write pulses. There is a significant change in resistance with almost no perceivable change in sample topography.

The electrical conduction behaviour, field-induced switching and electrothermal resistance drop due to atomic rearrangement indicate strong similarities with phase-change materials. This also reveals the potential of a-C as a similar nonvolatile memory candidate material.

Acknowledgments

The authors acknowledge contributions from several past and present colleagues from IBM Research—Zurich, in particular D Caimi, P Bächtold, W Häberle, A Pantazi, H Bhaskaran, R Cannara and S Karg. We would like to thank K Virwani from IBM Research—Almaden for assistance with c-AFM measurements of laser-heated samples. We would also like to thank C Bolliger for assistance with the preparation of the manuscript. Part of this work was performed at the Swiss Light Source, Paul Scherrer Institut, Villigen, Switzerland.

References

[1] Rueckes T, Kim K, Joselevich E, Tseng G Y, Cheung C-L and Lieber C M 2000 Carbon nanotube based nonvolatile random access memory for molecular computing *Science* **289** 94–7
[2] Li Y, Sinitskii A and Tour J M 2008 Electronic two-terminal bistable graphitic memories *Nat. Mater.* **7** 966–71
[3] Standley B, Bao W, Zhang H, Bruck J, Lau C N and Bockrath M 2008 Graphene-based atomic-scale switches *Nano Lett.* **8** 3345–9
[4] Wuttig M and Yamada N 2007 Phase-change materials for rewritable data storage *Nat. Mater.* **6** 824–32
[5] Meijer G I 2008 Who wins the nonvolatile memory race? *Science* **319** 1625–6

[6] Robertson J 2002 Diamond-like amorphous carbon *Mater. Sci. Eng.* **37** 129–81
[7] Silva S R P 2003 *Properties of Amorphous Carbon* 1st edn (Stevenage: The Institution of Engineering and Technology)
[8] Takai K, Oga M, Sato H, Enoki T, Ohki Y, Taomoto A, Suenaga K and Iijima S 2003 Structure and electronic properties of a nongraphitic disordered carbon system and its heat-treatment effects *Phys. Rev.* B **67** 214202
[9] Ferrari A C, Kleinsorge B, Morrison N A, Hart A, Stolojan V and Robertson J 1999 Stress reduction and bond stability during thermal annealing of tetrahedral amorphous carbon *J. Appl. Phys.* **85** 7191–7
[10] Grierson D S, Sumant A V, Konicek A R, Friedmann T A, Sullivan J P and Carpick R W 2010 Thermal stability and rehybridization of carbon bonding in tetrahedral amorphous carbon *J. Appl. Phys.* **107** 033523
[11] Mercer T W, DiNardo N J, Rothman J B, Siegal M P, Friedmann T A and Martinez-Miranda L J 1998 Electron emission induced modifications in amorphous tetrahedral diamondlike carbon *Appl. Phys. Lett.* **72** 2244–6
[12] Ronning C, Griesmeier U, Gross M, Hoffsäss H C, Downing R G and Lamaze G P 1995 Conduction processes in boron-nitrogen-doped diamond-like carbon films prepared by mass-separated ion beam deposition *Diam. Relat. Mater.* **4** 666–72
[13] Liu S, Lamp D, Gangopadhyay S, Sreenivas G, Ang S S and Naseem H A 1998 A new metal-to-metal antifuse with amorphous carbon *IEEE Electron Device Lett.* **19** 317
[14] Tsuchitani S, Isozaki M, Kaneko R, Tanaka I and Hirono S 2004 Nanometer-scale recording on a superhard and conductive carbon film using an atomic force microscope *Japan. J. Appl. Phys.* **43** 7677–81
[15] Kostylev S, Lowrey T and Czubatyj W 2007 Programming speed in ovonic unified memory *Proc. of the European Phase Change and Ovonics Symp.*
[16] Kreupl F *et al* 2008 Carbon-based resistive memory *IEEE Int. Electron Devices Meeting Technical Digest* pp 521–4
[17] Bhaskaran H, Sebastian A and Despont M 2009 Nanoscale PtSi tips for conducting probe technologies *IEEE Trans. Nanotechnol.* **8** 128–31
[18] Bhaskaran H, Sebastian A, Pauza A, Pozidis H and Despont M 2009 Nanoscale phase transformation in $Ge_2Sb_2Te_5$ using encapsulated scanning probes and retraction force microscopy *Rev. Sci. Instrum.* **80** 083701
[19] Adkins C J, Freake S M and Hamilton E M 1970 Electrical conduction in amorphous carbon *Phil. Mag.* **22** 183–8
[20] Khan R U A and Silva S R P 2000 Electronic conduction in ion implanted amorphous carbon thin films *Int. J. Mod. Phys.* B **14** 195–2005
[21] Balachova O V, Swart J W, Braga E S and Cescato L 2001 Permittivity of amorphous hydrogenated carbon (a-C:H) films as a function of thermal annealing *Microelectron. J.* **32** 673–8
[22] Ielmini D and Zhang Y 2007 Analytical model for subthreshold conduction and threshold switching in chalcogenide-based memory devices *J. Appl. Phys.* **102** 054517
[23] Adler D, Shur M S, Silver M and Ovshinsky S R 1980 Threshold switching in chalcogenide-glass thin films *J. Appl. Phys.* **51** 3289–309
[24] Pirovano A, Lacaita A L, Benvenuti A, Pellizer F and Bez R 2004 Electronic switching in phase-change memories *IEEE Trans. Electron. Devices* **51** 452–9
[25] Miyajima Y, Adikaari A A D T, Henley S J, Shannon J M and Silva S R P 2008 Electrical properties of pulsed UV laser irradiated amorphous carbon *Appl. Phys. Lett.* **92** 152104
[26] Ferrari A C and Robertson J 2000 Interpretation of Raman spectra of disordered and amorphous carbon *Phys. Rev.* B **61** 14095
[27] Pires D, Hedrick J L, Silva De A, Frommer J, Gotsmann B, Wolf H, Despont M, Duerig U and Knoll A W 2010 Nanoscale three-dimensional patterning of molecular resists by scanning probes *Science* **328** 732–5
[28] Guisinger N P and Arnold M S 2010 Beyond silicon: carbon-based nanotechnology *MRS Bull.* **35** 273–9
[29] Wright C D, Shah P, Wang L, Aziz M M, Sebastian A and Pozidis H 2010 Write strategies for multiterabit per square inch scanned-probe phase-change memories *Appl. Phys. Lett.* **97** 173104
[30] Pantazi A *et al* 2008 Probe-based ultrahigh-density storage technology *IBM J. Res. Dev.* **52** 493–511